



HAL
open science

Mechanical behavior of moderately inflated tubular organs: a three-dimensional analytical approach

Agnès Drochon

► **To cite this version:**

Agnès Drochon. Mechanical behavior of moderately inflated tubular organs: a three-dimensional analytical approach. 2024. hal-04760209

HAL Id: hal-04760209

<https://utc.hal.science/hal-04760209v1>

Preprint submitted on 30 Oct 2024

HAL is a multi-disciplinary open access archive for the deposit and dissemination of scientific research documents, whether they are published or not. The documents may come from teaching and research institutions in France or abroad, or from public or private research centers.

L'archive ouverte pluridisciplinaire **HAL**, est destinée au dépôt et à la diffusion de documents scientifiques de niveau recherche, publiés ou non, émanant des établissements d'enseignement et de recherche français ou étrangers, des laboratoires publics ou privés.



Distributed under a Creative Commons Attribution 4.0 International License

Mechanical behavior of moderately inflated tubular organs: a three-dimensional analytical approach

Agnès Drochon ^{1,2}

1. Univ. Bordeaux, CNRS, Bordeaux INP, I2M, UMR 5295, F-33400 Talence, France
2. Arts et Métiers Institute of Technology, CNRS, Bordeaux INP, I2M, UMR 5295, F-33400 Talence, France
Email: agnes.drochon@u-bordeaux.fr

How to cite this paper: Agnès Drochon (2024) Mechanical behavior of moderately inflated tubular organs: a three-dimensional analytical approach. *****, *, *-*, https://dx.doi.org/10.4236/**.2024.****

Received: **** **, **
Accepted: **** **, **
Published: **** **, **

Copyright © 2020 by author(s) and Scientific Research Publishing Inc. This work is licensed under the Creative Commons Attribution International License (CC BY 4.0).
<http://creativecommons.org/licenses/by/4.0/>



Open Access

Abstract

Hollow tubular tissues and organs of our body have various functions : gastrointestinal (esophagus), respiratory (trachea), vascular (veins, arteries). A panel of pathologies is associated with each of these tissues and therapeutic interventions, surgery or replacement may be necessary. A precise knowledge of the mechanical properties of these tissues is thus required in order to understand their functioning in native conditions, to be able to elaborate some prostheses, or to design appropriate surgical training tools. These tissues may undergo expansions or contractions (peristalsis) and are exposed to internal pressures. The wall of tubular organs is organized in different layers, and each layer consists of various cell types and extra-cellular matrix, depending on the physiological functions that the organ has to fulfil. This yields anisotropic and compliant structures. In inflation experiments, the linear elasticity approach is acceptable as long as the organ's inflation remains moderate. In this paper, elasticity laws are revisited and supplemented in order to show that, coupled with modern experimental characterization tools, they provide useful informations (**compliances, directional Young moduli, Poisson ratios**) for the design of artificial tubular organs. The importance of a precise determination of the wall thickness and of its evolution during inflation is pointed out.

Keywords

Tubular organs, inflation experiments, linear elasticity, anisotropy, Young modulus, Poisson's coefficients

1. Introduction

Since the 1960s, the linear elasticity theory has been widely used to analyse inflation experiments performed with blood vessels or vascular biomaterials (a

non-specialist reader can consult for example the resource book of Y.C. Fung [1]). Vessel walls must have enough strength in the circumferential direction to withstand arterial pressures and enough compliance to allow pulsatile flow. Classical mechanical tests consist of longitudinal or circumferential tensile tests and inflation experiments. In some studies, ultimate tensile strength, elongation at break and suture retention force are also measured. The most straightforward informations deduced from inflation experiments are the compliance of the organ's wall (relative increase in diameter consecutive to a given increase in internal pressure) and the burst pressure. In order to infer more detailed mechanical parameters, a constitutive law for the wall is necessary. Linear elasticity approach is acceptable as long as the deformations remain small (corresponding to the linear part of the stress-strain curve). If the material is assumed isotropic, it is possible to infer its Young's modulus (E) and Poisson ratio (ν) from tube equilibrium equations [2]. However, the structural organization (layered microstructure composed of collagen, elastin, and SMCs (smooth muscle cells)) of vessels walls confers to them some anisotropic properties [3, 4]. Mechanical responses to some solicitation are not the same in any directions. The studies of Dobrin and Doyle [5], Dobrin [6], Lillie et al. [7] provide calculations for circumferential and longitudinal elastic modulus, based on the assumption that the radial stress (the stress which tends to compress the wall) amounts to only a few percents of the longitudinal and azimuthal stress. For that reason, they neglect *a priori* the σ_r contribution in their analysis.

Concomitantly, mechanical tests were also performed on vascular grafts in order to check the graft patency. Some compliance mismatch between the graft and the host artery may lead to graft thrombosis [8, 9]. Dynamic compliance can be evaluated as $((D_s - D_d)/D_d)/(P_s - P_d)$ where subscripts s and d mean « systolic » and « diastolic », D is the graft diameter, and P the internal pressure. Circumferential compliance allows the prosthesis to expand in response to the pulsatile pressure. The trend is to optimize materials and tubular bio-structures before surgery [10, 11]. Many other motivations may be cited: modeling arterial clamping or balloon dilatation, helping understanding pathologies and improving treatments, fabrication of manikins for medical training or adaptation to robotic surgery.

More recently, other tubular organs have also been studied, such as esophagus or trachea. A detailed description of these organs and of their physiological functions in relation with their mechanical requirements may be found in the reviews of Pien et al. [4] and of Saksena et al. [12]. These organs may be affected by a variety of diseases or injuries: congenital malformation, autoimmune disease, inflammation, infection, cancer. Resection and replacement is sometimes unavoidable, and may be associated with other problems (leakage, rejection, stricture). The esophagus has to be compliant enough in order to convey food to the stomach by peristalsis and contractions of the muscle layer. The trachea is submitted to air pressure variations during the respiratory cycle (inspiration / expiration). Two recent review papers are focused more precisely on the gastrointestinal tissues [13, 14]. They point out the anisotropy of these tissues due to their multi-layered structure and indicate that inflation-extension tests may be appropriate to characterize both the distension of the tissue in the circumferential direction and the stretch in the longitudinal direction.

Many groups now use tissue engineering technologies to fabricate synthetic constructs as tissue replacements of hollow tubular organs. Several review papers

give an extensive description of the fabrication processes (scaffolds, cells, mechanical and biological tests required for the regenerated organ) [3, 4, 12, 15]. Mechanical and biological performances are closely linked since the scaffold stiffness influences cell-material interactions and cell differentiation. In view of implantation, anatomical accuracy, suturability, autoimmune acceptance, long-term patency are also required for the tubular constructs. Bio-engineered tubular organs may also be used for fundamental research: basic science, better understanding of some disease, drug testing. Examples of organ targeted studies may be found in De Mel et al. [16] (3D tubular scaffolds for paediatric organ production), Farhat et al. [17] (3D bioprinting for esophageal tissue repair and reconstruction), Lee et al. [18] (3D printing of vascularized tissues). In each case, the mechanical properties of the tubular structures are checked to match those of the human tissues.

Besides, noticeable progresses have been done with experimental characterizing tools that allow three-dimensional measurements of local strains and stresses. Bernal et al. [19] proposed a technique that uses sonometry data from piezoelectric elements to measure the strain in the longitudinal and circumferential directions of pressurized arteries. A review by Macrae et al. [20] is especially dedicated to « methods in mechanical testing of arterial tissues ». In addition to improved optical measuring systems, marker tracking, CT scan or electronic speckle pattern interferometry are quoted as techniques that allow to evaluate stresses and strains. Sanders et al. [21] used ultrasound strain imaging in whole-vessel-inflation experiments. Strain maps were obtained through intravascular ultrasound elastography. They aimed at characterizing mechanical properties of the different atherosclerotic plaque constituents in order to evaluate the rupture risk of the plaque. An optical clearing method is adopted by Maeda et al. [22]. It is coupled with imaging and microscopy techniques and allows some three-dimensional characterization of the mechanical behavior of rat thoracic aorta under intraluminal pressurization. Microstructural analysis of the inflated tissue is provided. Urban et al. [23] demonstrate that the ultra-sound technique can be precise enough to capture the diameter variation of an artery due to the pressure pulse transmitted by blood flow. This allows to evaluate the compliance of the artery wall. In future works, they plan to use different US propagating modes in the axial and circumferential directions in order to capture anisotropic mechanical properties of the vessel wall.

In this context, elasticity laws are revisited and completed in this paper. **If coupled with microstructural measurements provided by modern experimental tools, the proposed three-dimensional analysis of the deformation of anisotropic tubular organs under moderate inflation can allow a more detailed comprehension of the mechanical behavior of native and fabricated tissues.**

2. Theoretical methodology

Let us consider a hollow tubular organ with the following known initial dimensions: wall thickness h_0 , external diameter d_{e0} , ($d_{e0} = 2 r_{e0}$), length l_0 . Classical cylindrical coordinates (r, θ, z) are used, and z is the longitudinal axis (Fig.1). If an internal pressure P is applied inside the tube (the external pressure is taken as zero), its diameter will increase due to the compliance of the wall.

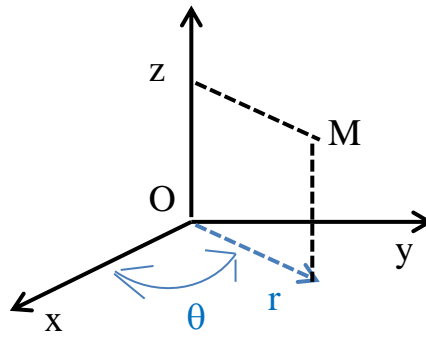


Figure 1. Cylindrical coordinates.

This increase in diameter is associated with a decrease in wall thickness and a length variation. The dimensions in the deformed state are denoted h for the wall thickness, $d_e (= 2 r_e)$ for the diameter, and l for the length. (Fig.2)

The internal radii at time $t = 0$ are easily obtained as :

$$r_{i0} = r_{e0} - h_0 \tag{1}$$

The initial cross section of the esophagus wall is :

$$S_0 = \pi (r_{e0}^2 - r_{i0}^2) \tag{2}$$

Wall incompressibility [24, 25] yields :

$$\pi (r_e^2 - r_i^2) l = \pi (r_{e0}^2 - r_{i0}^2) l_0 \tag{3}$$

The deformed internal radius r_i is deduced from this wall volume conservation. Then the deformed wall thickness, h , may be evaluated as:

$$h = r_e - r_i \tag{4}$$

The initial volume of the esophagus is:

$$V_0 = \pi r_{e0}^2 l_0 \tag{5}$$

and its volume in the inflated state is :

$$V = \pi r_e^2 l \tag{6}$$

Tubular organ cross-section

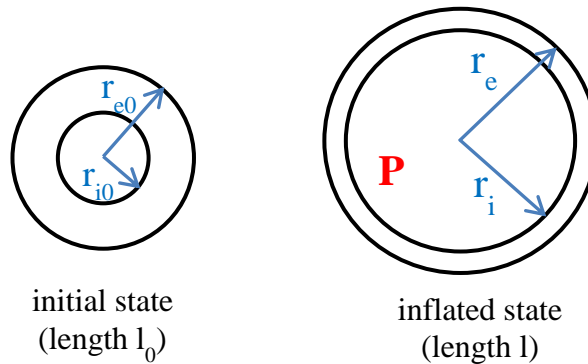


Figure 2. Tubular organ geometry in the initial state and under internal pressure P .

This allows to calculate a compliance, based on the relative volume variation in response to the imposed internal pressure P :

$$C_v = \frac{\left(\frac{V-V_0}{V_0}\right)}{P} \quad (7).$$

The inverse of C_v ($E_p = 1 / C_v$) may be interpreted as a « pressure elastic modulus ». A compliance based on diameter variation, C_d , may also be defined :

$$C_d = \frac{\left(\frac{d_e-d_{e0}}{d_{e0}}\right)}{P} \quad (8).$$

However, these compliances C_d and C_v do not account for the changes in wall thickness [26]. A possible length variation during inflation is taken into account in C_v , but not in C_d .

A three-dimensional analysis may be proposed as follows:

Classical notations in a cylindrical frame are used for the extension ratios : $\lambda_z = l/l_0$ is the longitudinal extension ratio ; $\lambda_\theta = d_e / d_{e0}$ is the circumferential extension ratio (perimeter of the inflated tube / perimeter of the initial tube) and $\lambda_r = h/h_0$ is the radial stretch ratio (change of dimension in the radial direction). As explained by Patel et al. [27] and Dobrin and Doyle [5], only orthogonal elongating strains in the three principal geometric directions need to be considered when the tubular sample is loaded by inflation and longitudinal traction.

The corresponding deformations are denoted e_{rr} , $e_{\theta\theta}$, and e_{zz} , with

$$e_{rr} = \lambda_r - 1, \quad e_{\theta\theta} = \lambda_\theta - 1, \quad e_{zz} = \lambda_z - 1 \quad (9).$$

We adopt the following approached formulas in order to compute the stresses in the esophagus wall:

- The radial normal stress, σ_{rr} , is estimated as: $\sigma_{rr} = -P/2$ (10)

(This is the mean value between the internal pressure P , and the external pressure (0)).

- The circumferential stress, $\sigma_{\theta\theta}$, is : $\sigma_{\theta\theta} = P \frac{r_i}{h}$ (11)

The longitudinal stress, σ_{zz} , is calculated as the sum of two components :

$$\sigma_{zz} = \frac{P \pi r_i^2}{\pi (r_e^2 - r_i^2)} + \sigma_{zext} \quad (12),$$

where the first term corresponds to the longitudinal stress due to pressure and the second term (σ_{zext}) is the stress due to an eventual external longitudinally applied traction.

These formulas have been widely used for inflated elastic tissues (for example, blood vessels) [5, 6, 7, 27]. They rely on the assumptions that the wall thickness h is small when compared to the vessel radius r , and that σ_{rr} varies linearly across the wall. They were initially deduced from the equations describing the equilibrium of an isotropic inflated elastic tube, that are recalled in [10]. As explained above, in such inflation experiments, shear stresses and shear deformations are classically neglected [19].

Constitutive equations for static anisotropic elasticity may be derived from the paper of Patel et al. [27]:

$$\begin{pmatrix} e_{rr} \\ e_{\theta\theta} \\ e_{zz} \end{pmatrix} = \begin{pmatrix} 1/E_r & -\nu_{r\theta}/E_\theta & -\nu_{rz}/E_z \\ -\nu_{\theta r}/E_r & 1/E_\theta & -\nu_{\theta z}/E_z \\ -\nu_{zr}/E_r & -\nu_{z\theta}/E_\theta & 1/E_z \end{pmatrix} \begin{pmatrix} \sigma_{rr} \\ \sigma_{\theta\theta} \\ \sigma_{zz} \end{pmatrix} \quad (13),$$

where E_r (Pa), E_θ (Pa) and E_z (Pa) denote the elastic moduli in the radial, circumferential and longitudinal directions.

Due to symmetry conditions, some additional relations exist:

$$\frac{\nu_{z\theta}}{E_\theta} = \frac{\nu_{\theta z}}{E_z} ; \frac{\nu_{zr}}{E_r} = \frac{\nu_{rz}}{E_z} ; \frac{\nu_{r\theta}}{E_\theta} = \frac{\nu_{\theta r}}{E_r} \quad (14).$$

The quantities $\nu_{r\theta}$, ν_{rz} , $\nu_{\theta z}$, $\nu_{\theta r}$, ν_{zr} , $\nu_{z\theta}$ are Poisson ratios. For example, $\nu_{r\theta}$ represents the ratio of the contractile strain in the radial direction due to an elongating strain in the circumferential direction, ν_{rz} represents the ratio of the contractile strain in the radial direction due to an elongating strain in the longitudinal direction, etc... More generally, ν_{ij} characterize the strain in the i -direction produced by a loading in the j -direction.

The incompressibility of the tissue imposes the following condition :

$$e_{rr} + e_{\theta\theta} + e_{zz} = 0 \quad (15).$$

The condition (15) may be expressed using the equations (13).

This writes:

$$\frac{\sigma_{rr}}{E_r} - \frac{\nu_{r\theta}}{E_\theta} \sigma_{\theta\theta} - \frac{\nu_{rz}}{E_z} \sigma_{zz} - \frac{\nu_{\theta r}}{E_r} \sigma_{rr} + \frac{\sigma_{\theta\theta}}{E_\theta} - \frac{\nu_{\theta z}}{E_z} \sigma_{zz} - \frac{\nu_{zr}}{E_r} \sigma_{rr} - \frac{\nu_{z\theta}}{E_\theta} \sigma_{\theta\theta} + \frac{\sigma_{zz}}{E_z} = 0 \quad (16);$$

that is:

$$\frac{\sigma_{rr}}{E_r} (1 - \nu_{\theta r} - \nu_{zr}) + \frac{\sigma_{\theta\theta}}{E_\theta} (1 - \nu_{r\theta} - \nu_{z\theta}) + \frac{\sigma_{zz}}{E_z} (1 - \nu_{rz} - \nu_{\theta z}) = 0 \quad (17)$$

In order that Eq.17 can be satisfied in any case, the factor of σ_{rr} / E_r in this sum has to be nul, idem for the factor of $\sigma_{\theta\theta}/E_\theta$, and the factor of σ_{zz} / E_z . Consequently,

$$\begin{cases} \nu_{\theta r} + \nu_{zr} = 1 \\ \nu_{r\theta} + \nu_{z\theta} = 1 \\ \nu_{rz} + \nu_{\theta z} = 1 \end{cases} \quad (18)$$

or equivalently (using (14)):

$$\begin{cases} \nu_{r\theta} \frac{E_r}{E_\theta} + \nu_{rz} \frac{E_r}{E_z} = 1 \\ \nu_{r\theta} + \nu_{\theta z} \frac{E_\theta}{E_z} = 1 \\ \nu_{rz} + \nu_{\theta z} = 1 \end{cases} \quad (19).$$

The Poisson coefficients $\nu_{r\theta}$, ν_{rz} , and $\nu_{\theta z}$ thus depend on the orthogonal elastic moduli and may be deduced from the system of equations (19) :

$$\nu_{rz} = \frac{1}{2} - \frac{1}{2} E_z \left(\frac{1}{E_\theta} - \frac{1}{E_r} \right) \quad (20)$$

$$\nu_{r\theta} = \frac{1}{2} - \frac{1}{2} E_\theta \left(\frac{1}{E_z} - \frac{1}{E_r} \right) \quad (21)$$

$$\nu_{\theta z} = \frac{1}{2} - \frac{1}{2} E_z \left(\frac{1}{E_r} - \frac{1}{E_\theta} \right) \quad (22)$$

and then

$$\nu_{\theta r} = \frac{1}{2} - \frac{1}{2} E_r \left(\frac{1}{E_z} - \frac{1}{E_\theta} \right) \quad (23)$$

$$\nu_{zr} = \frac{1}{2} - \frac{1}{2} E_r \left(\frac{1}{E_\theta} - \frac{1}{E_z} \right) \quad (24)$$

$$\nu_{z\theta} = \frac{1}{2} - \frac{1}{2} E_\theta \left(\frac{1}{E_r} - \frac{1}{E_z} \right) \quad (25).$$

One can notice that :

$$\frac{1}{6} (v_{r\theta} + v_{rz} + v_{\theta z} + v_{\theta r} + v_{zr} + v_{z\theta}) = \frac{1}{2} \quad (26),$$

and that Eq. (22) is also given in Lillie et al. [7], with the physical meaning of “ a decrease in radius obtained on increase in length under uniaxial load”. Equations (20) to (25) thus develop and confirm the approach initiated by Patel et al.[27].

In the case of isotropy $E_r = E_\theta = E_z$ and, as expected for an incompressible material,

$$v_{r\theta} = v_{rz} = v_{\theta z} = v_{\theta r} = v_{zr} = v_{z\theta} = \frac{1}{2} .$$

Equation (13) coupled with equations (20) to (25) can be re-written as follows:

$$\begin{cases} e_{rr} = \frac{1}{E_r} \sigma_{rr} - \sigma_{\theta\theta} \left(\frac{1}{2E_\theta} - \frac{1}{2E_z} + \frac{1}{2E_r} \right) - \sigma_{zz} \left(\frac{1}{2E_z} - \frac{1}{2E_\theta} + \frac{1}{2E_r} \right) \\ e_{\theta\theta} = -\sigma_{rr} \left(\frac{1}{2E_\theta} - \frac{1}{2E_z} + \frac{1}{2E_r} \right) + \frac{1}{E_\theta} \sigma_{\theta\theta} - \sigma_{zz} \left(\frac{1}{2E_z} - \frac{1}{2E_r} + \frac{1}{2E_\theta} \right) \\ e_{zz} = -\sigma_{rr} \left(\frac{1}{2E_z} - \frac{1}{2E_\theta} + \frac{1}{2E_r} \right) - \sigma_{\theta\theta} \left(\frac{1}{2E_z} - \frac{1}{2E_r} + \frac{1}{2E_\theta} \right) + \frac{1}{E_z} \sigma_{zz} \end{cases} \quad (27)$$

The relative deformations e_{rr} , $e_{\theta\theta}$, e_{zz} can be deduced from the experiments (Eq. 9) ; the normal stresses σ_{rr} , $\sigma_{\theta\theta}$, and σ_{zz} can be estimated using Eq. (10) to (12).

One may introduce the quantities : $X_r = 1/E_r$, $X_\theta = 1/E_\theta$, and $X_z = 1/E_z$. . The system to solve thus becomes:

$$\begin{cases} 2e_{rr} = X_r (2\sigma_{rr} - \sigma_{\theta\theta} - \sigma_{zz}) + (\sigma_{zz} - \sigma_{\theta\theta}) X_\theta - (\sigma_{zz} - \sigma_{\theta\theta}) X_z \\ 2e_{\theta\theta} = (\sigma_{zz} - \sigma_{rr}) X_r + X_\theta (-\sigma_{rr} + 2\sigma_{\theta\theta} - \sigma_{zz}) - (\sigma_{zz} - \sigma_{rr}) X_z \\ 2e_{zz} = -(\sigma_{rr} - \sigma_{\theta\theta}) X_r + (\sigma_{rr} - \sigma_{\theta\theta}) X_\theta + X_z (-\sigma_{rr} - \sigma_{\theta\theta} + 2\sigma_{zz}) \end{cases} \quad (28)$$

Since the 3 equations of this system are linked by the relation: $e_{rr} + e_{\theta\theta} + e_{zz} = 0$, one of the unknown has to be taken as a parameter or determined by another method (for example traction experiments performed with the studied tissue samples). If we suppose that the longitudinal modulus, E_z , is known, X_r and X_θ are deduced from (Eq.28) and expressed as functions of e_{rr} , $e_{\theta\theta}$, and X_z .

$$X_r = \frac{1}{E_r} = e_{rr} \frac{(\sigma_{rr} - 2\sigma_{\theta\theta} + \sigma_{zz})}{(\sigma_{rr} - \sigma_{\theta\theta})^2} + e_{\theta\theta} \frac{(\sigma_{zz} - \sigma_{\theta\theta})}{(\sigma_{rr} - \sigma_{\theta\theta})^2} + X_z \frac{(\sigma_{zz} - \sigma_{\theta\theta})^2}{(\sigma_{rr} - \sigma_{\theta\theta})^2} \quad (29)$$

$$X_\theta = \frac{1}{E_\theta} = e_{rr} \frac{(\sigma_{zz} - \sigma_{rr})}{(\sigma_{rr} - \sigma_{\theta\theta})^2} - e_{\theta\theta} \frac{(2\sigma_{rr} - \sigma_{\theta\theta} - \sigma_{zz})}{(\sigma_{rr} - \sigma_{\theta\theta})^2} + X_z \frac{(\sigma_{rr} - \sigma_{zz})^2}{(\sigma_{rr} - \sigma_{\theta\theta})^2} \quad (30)$$

Coming back to Eq. (20) to (25), it is then possible to calculate all the Poisson coefficients.

3. Illustrative example with literature data

Intraluminal pressurization of rat thoracic aorta is considered. The data are taken from Maeda et al. [22]. The specimen initial geometry is $h_0 = 150 \mu\text{m}$, $r_{e0} = 1 \text{ mm}$, $l_0 = 20 \text{ mm}$ (so that the initial internal radius $r_{i0} = 0.85 \text{ mm}$). For an internal pressure $P = 40 \text{ mmHg}$, the deformations $e_{\theta\theta}$ and e_{zz} are reported as: $e_{\theta\theta} = 0.26$ and $e_{zz} = 0.008$. It is thus possible to calculate the deformed geometry: $r_e = 1.26 \text{ mm}$, $r_i = 1.146 \text{ mm}$, $h = 114.3 \mu\text{m}$. These geometric data are summarized in Table1.

Table 1. Specimen geometry (Ref [22] is the data source)

| | Internal radius r_i (mm) | External radius r_e (mm) | Thickness (μm) | Length (mm) |
|------------------|----------------------------|----------------------------|-----------------------------|-------------|
| Before inflation | 0.85 | 1 | 150 | 20 |
| Inflated | 1.146 | 1.26 | 114.3 | 20.16 |

Table 2. Stresses calculated with measurements from [22]

| σ_{rr} (Pa) | $\sigma_{\theta\theta}$ (Pa) | σ_{zz} (Pa) |
|--------------------|------------------------------|--------------------|
| -2667 | 53458 | 25459 |

Table 3. Young moduli calculated with measurements from [22]

| E_r (Pa) | E_θ (Pa) | E_z (Pa) (from [25]) |
|-------------------|-------------------|------------------------|
| $1.53 \cdot 10^5$ | $1.36 \cdot 10^5$ | $1 \cdot 10^5$ |

Table 4. Poisson coefficients calculated with measurements from [22]

| ν_{rz} | $\nu_{r\theta}$ | $\nu_{\theta z}$ | $\nu_{\theta r}$ | ν_{zr} | $\nu_{z\theta}$ |
|------------|-----------------|------------------|------------------|------------|-----------------|
| 0.459 | 0.264 | 0.54 | 0.296 | 0.7 | 0.736 |

The volume compliance (Eq. (7)) is $1.12 \cdot 10^{-4} \text{ Pa}^{-1}$ and the diameter compliance (Eq. (8)) is $4.87 \cdot 10^{-5} \text{ Pa}^{-1}$. The radial stretch ratio λ_r is 0.762 so that $e_{rr} = -0.238$. The stresses are obtained through Eq. (10-12) and are summarized in Table 2. It is observed that, as expected, $\sigma_{\theta\theta} \approx 2 \sigma_{zz}$. The radial stress (the stress which tends to compress the wall) amounts to only 10 % of the longitudinal stress and 5% of the azimuthal stress. For that reason, some authors [5, 7, 28] neglect *a priori* the σ_{rr} contribution in their analysis. Using the value of Assoul et al. [25] for the longitudinal elastic modulus E_z of the rat thoracic aorta ($E_z = 1 \cdot 10^5 \text{ Pa}$), the radial and circumferential elastic moduli are deduced from Eq. (29) and (30): $E_r = 1.53 \cdot 10^5 \text{ Pa}$, and $E_\theta = 1.36 \cdot 10^5 \text{ Pa}$. These results are summarized in Table 3. The corresponding Poisson coefficients (Eq. (20-25)) are presented in Table 4.

No sophisticated interpretation of these results can be made because they are based on rough estimations of the input data. However, the orders of magnitude are in good agreement with similar results that can be found in the literature. Cox [29] studied the anisotropic properties of the canine carotid artery with significant axial pre-stress ($\lambda_z > 1.5$) and pressures up to 200 mmHg. He mentions that the elastic moduli (in the range $10^5 - 10^6 \text{ Pa}$) and the various Poisson ratios (between 0 and 1) are complex functions of the extension ratios. For the elastic moduli of aortas (estimated in living dogs), Patel et al. [27] report values in the range $3.9 \cdot 10^5 \text{ Pa}$ to $8.8 \cdot 10^5 \text{ Pa}$, with $E_r < E_\theta$ and E_z , depending on the extension ratio values (λ_θ and λ_z varying between 1.4 and 1.6). Nahon et al. [28] examined the mechanical properties of canine iliac arteries under operating pressures of 80 to 160 mmHg. Their approach is two-dimensional. For an internal pressure of 80 mmHg, they obtain $E_\theta = 2 \cdot 10^5 \text{ Pa}$, $E_z = 4.6 \cdot 10^5 \text{ Pa}$ and $\nu_{\theta z} = 0.56$. They also indicate a compliance value of $2.25 \cdot 10^{-5} \text{ Pa}^{-1}$ for some canine femoral artery. More recently, an attempt was made by Sugita et al. [30] to evaluate 3D local strains (at the cell scale) in mice thoracic aortas during intraluminal pressurization. In their work, one can also find an estimation of the volume compliance of the studied vessels around $0.37 \cdot 10^{-4} \text{ Pa}^{-1}$. Skacel and Bursa [31] tried to establish some relations between the Poisson

ratios and the internal layered structure of the arteries walls. Their demonstration is based on uniaxial traction experiments of porcine aortic wall. They show that “in-plane” Poisson ratios are between 0 and 0.5 and “out-of-plane” Poisson ratios can get values between 0.5 and 1. They also point out the importance of the transversal contraction (in the thickness direction).

4. Discussion

i) It may be of interest to evaluate if the assumption of isotropy in the analysis of inflation experiments would yield very different results. If the mechanical properties are supposed to be identical in all directions, the incompressibility condition leads to a value of 0.5 for ν , and the Young’s modulus may be found in Bergel [2]:

$$E_B = \frac{\Delta P}{\left(\frac{\Delta r_e}{r_{e0}}\right)} \frac{2(1-\nu^2)r_i^2}{(r_e^2 - r_i^2)} \quad (31)$$

This equation is established with the hypothesis that no change in length occurs during the inflation experiment. Since $\nu = 0.5$, Equ. (31) becomes:

$$E_B = \frac{\Delta P}{\left(\frac{\Delta r_e}{r_{e0}}\right)} \frac{3r_i^2}{2(r_e^2 - r_i^2)} \quad (32)$$

A change in length Δl may be easily taken into account as a boundary condition in the longitudinal displacement. This leads to the following formula for the elastic modulus :

$$E_{Bmodified} = \frac{\Delta P}{\left(\frac{\Delta r_e}{r_{e0}} + \nu \frac{\Delta l}{l_0}\right)} \frac{2(1-\nu^2)r_i^2}{(r_e^2 - r_i^2)} \quad (33)$$

One can notice that if $\Delta l = 0$, Eq. (33) reduces to Eq. (31). Using the notations of this paper, $\Delta P = P - P_0$, $\Delta r_e / r_{e0} = e_{\theta\theta}$, and $\Delta l / l_0 = e_{zz}$.

The E_B modulus as defined in Eq. (31) may be closely related to a circumferential modulus, since it is inversely proportional to the wall compliance C_d (Eq.8) and proportional to a geometric factor of order (r_i / h) :

$$E_B = \frac{1}{c_d} \frac{2(1-\nu^2)r_i^2}{(r_e - r_i)(r_e + r_i)} \approx \frac{1}{c_d} \frac{(1-\nu^2)r_i}{h} \quad (34)$$

With the numerical data adopted in Section 3, the value of E_B from Eq. (32) is $1.47 \cdot 10^5$ Pa and the value from Eq. (34) is $1.54 \cdot 10^5$ Pa. Both values are close to the E_0 value obtained in Section 3 ($E_0 = 1.36 \cdot 10^5$ Pa).

ii) If internal pressures and tube radii are increased further, the linear elasticity approach is no more valid. The stiffness of the tissue increases with the load, and this produces an exponential stress-strain relationship. Different models have been proposed in the literature to describe this hyperelastic behavior. One of the most popular is the “HGO-model” [32].

5. Conclusion

In spite of the simplifying hypotheses that are made, the theoretical approaches presented in this paper may be useful for the interpretation of inflation experiments of tubular elastic biological tissues. Inflation induces deformations of the organ’s wall in the three directions (radial, circumferential, longitudinal). Each deformation influences the two others. The Poisson ratios are the physical quantities that

put in evidence this coupling. This paper stresses the importance of analyzing the evolution of the wall thickness during inflation and suggests the possibility to combine mechanical results with very detailed microscopic or imaging results.

Declaration of competing interest: No competing interest to declare.

Funding sources: No funding source to declare.

Ethical approval: Not required

ORCID number Agnès DROCHON:

<https://orcid.org/0000-0001-8220-5189>

References

- [1] Fung, Y.C. (1993) *Biomechanics: mechanical properties of living tissues*. Springer (2nd ed.), New York.
- [2] Bergel, D. (1961) The static elastic properties of the arterial wall. *J. Physiol.* **156** : 445-457. doi: [10.1113/jphysiol.1961.sp006686](https://doi.org/10.1113/jphysiol.1961.sp006686)
- [3] Boys, A., Barron, S., Tilev, D., and Owens, R. (2020) Building Scaffolds for Tubular Tissue Engineering. *Front Bioeng Biotechnol.* **8**: 589960. doi: [10.3389/fbioe.2020.589960](https://doi.org/10.3389/fbioe.2020.589960)
- [4] Pien, N., Palladino, S., Copes, F., Candiani, G., Dubruel, P., Van Vlierberghe, S., and Mantovani, D. (2022) Tubular bioartificial organs : from physiological requirements to fabrication processes and resulting properties. A critical review. *Cells, Tissues, Organs.* **211** : 420-446. DOI:[10.1159/000519207](https://doi.org/10.1159/000519207)
- [5] Dobrin, P. and Doyle, J. (1970) Vascular smooth muscle and the anisotropy of dog carotid artery. *Circulation Research*, Vol. **XXVII**: 105-119. DOI: [10.1161/01.res.27.1.105](https://doi.org/10.1161/01.res.27.1.105)
- [6] Dobrin, P. (1986) Biaxial anisotropy of dog carotid artery : estimation of circumferential elastic modulus. *J. Biomechanics*, **19** (5): 351-358. DOI: [10.1016/0021-9290\(86\)90011-4](https://doi.org/10.1016/0021-9290(86)90011-4)
- [7] Lillie, M., Shadwick, R. and Gosline, J. (2010) Mechanical anisotropy of inflated elastic tissue from the pig aorta. *Jour. Biomechanics*, **43**: 2070-2078. DOI: [10.1016/j.jbiomech.2010.04.014](https://doi.org/10.1016/j.jbiomech.2010.04.014)
- [8] Abbott, W., Megerman, J., Hasson, J., L'Italien, G. and Warnock, D. (1987) Effect of compliance mismatch on vascular graft patency. *Jour. Vascular Surgery*, **5** (2) :376-382. [https://doi.org/10.1016/0741-5214\(87\)90148-0](https://doi.org/10.1016/0741-5214(87)90148-0)
- [9] Li, C., Wang, F., Douglas, G., Zhang, Z., Guidoin, R. and Wang, L. (2017) Comprehensive mechanical characterization of PLA fabric combined with PCL to form a composite structure vascular graft . *Jour. Mech. Behavior of Biomed. Materials.* **69** : 39-49. <http://dx.doi.org/10.1016/j.jmbbm.2016.11.005>

- [10] Castillo-Cruz, O., Perez-Aranda, C., Gamboa, F., Cauich-Rodriguez, J., Mantovani, D. and Aviles, F. (2018) Prediction of circumferential compliance and burst strength of polymeric vascular grafts. *Jour. Mech. Behavior BioMedical Materials*. **79** : 332-340. <https://doi.org/10.1016/j.jmbbm.2017.12.031>
- [11] Camasao, D. and Mantovani, D. (2021) The mechanical characterization of blood vessels and their substitutes in the continuous quest for physiological-relevant performances. A critical review. *Materials Today Bio*. **10** : 100106. DOI: 10.1016/j.mtbio.2021.100106
- [12] Saksena, R., Gao, C., Wicox, M. and De Mel, A. (2016) Tubular organ epithelialisation *Jour. Tissue Engineering*, **7** : 1-16. DOI:10.1177/2041731416683950
- [13] Patel, B., Gizzi, A., Hashemi, J., Awakeem, Y., Gregersen, H. and Kassab, G. (2022) Biomechanical constitutive modeling of the gastrointestinal tissues: a systematic review. *Materials and Design*, **217**: 110576. <https://doi.org/10.1016/j.matdes.2022.110576>
- [14] Durcan, C., Hossain, M., Chagnon, G., Perié, D. and Girard, E. (2024) Mechanical experimentation of the gastrointestinal tract: a systematic review. *Biomechanics and Modeling in Mechanobiology*, **23** : 23-59. <https://doi.org/10.1007/s10237-023-01773-8>
- [15] Jeong, H., Nam, H., Jang, J. and Lee, S. (2020) 3D bioprinting strategies for the regeneration of functional tubular tissues and organs. *Bioengineering* **7**: 32. doi:10.3390/bioengineering7020032
- [16] De Mel, A., Yap, T., Cittadella, G., Hale, L., Maghsoudlou, P., De Coppi, P., et al. (2015) A potential platform for developing 3D tubular scaffolds for paediatric organ development. *J. Mater. Sci. Mater. Med.* **26(3)**:141. doi:10.1007/s10856-015-5477-4
- [17] Farhat, W., Chatelain, F., Marret, A., Faivre, L., Arakelian, L., Cattan, P. et al. (2021) Trends in 3D bioprinting for esophageal tissue repair and reconstruction. *Biomaterials* **267**: 120465. <https://doi.org/10.1016/j.biomaterials.2020.120465>
- [18] Lee, H., Jang, T., Han, G., Kim, H. and Jung, H (2021) Freeform 3D printing of vascularized tissues: challenges and strategies. *Jour Tissue Engineering* **12**:1-34. <https://doi.org/10.1177/20417314211057236>
- [19] Bernal, M., Urban, M., Rosario, D., Aquino, W. and Greenleaf, J. (2011) Measurement of biaxial mechanical properties of soft tubes and arteries using piezoelectric elements and sonometry. *Phys. Med. Biol.*, **56 (11)** : 3371-3386. DOI: 10.1088/0031-9155/56/11/012
- [20] Macrae, R., Miller, K. and Doyle, B. (2016) Methods in mechanical testing of arterial tissue : a review . *Strain*. doi :10.1111/str.12183
- [21] Sanders, S, Lopata, R., Van Breemen, L., Van de Vosse, F. and Rutten, M. (2020) A novel technique for the assessment of mechanical properties of vascular tissue » *Biomech. and Modeling in Mechanobio.*, **19** : 1585-1594. <https://doi.org/10.1007/s10237-020-01292-w>

- [22] Maeda, E., Ando, Y., Takeshita, K. and Matsumoto, T. (2022) Through the cleared aorta: three-dimensional characterization of mechanical behaviors of rat thoracic aorta under intraluminal pressurization using optical clearing method. *Nature Scientific Reports* **12**:8632. <https://doi.org/10.1038/s41598-022-12429-5>
- [23] Urban, M., Roy, T., Aquino, W., Guddati, M. and Greenleaf, J. (2023) Understanding arterial biomechanics with ultra-sound and waveguide - Models” *Acoustic Today*, **19(1)**: 46-54. [doi:10.1121/at.2023.19.1.46](https://doi.org/10.1121/at.2023.19.1.46)
- [24] Sommer, G., Schriefl, A., Zeindlinger, G., Katzensteiner, A., Ainödhofer, H., Saxena, A. et al. (2013) Multiaxial mechanical response and constitutive modeling of esophageal tissues: impact on esophageal tissue engineering. *Acta Biomaterialia*, **9(12)**: 9379-9391. [DOI: 10.1016/j.actbio.2013.07.041](https://doi.org/10.1016/j.actbio.2013.07.041)
- [25] Assoul, N., Flaud, P., Chaouat, M., Letourneur, D. and Bataille, I. (2008) Mechanical properties of rat thoracic and abdominal aortas. *J. Biomechanics*, **41**:2227-2236. [doi:10.1016/j.jbiomech.2008.04.017](https://doi.org/10.1016/j.jbiomech.2008.04.017)
- [26] Takeda, T., Kassab, G., Liu, J., Puckett, J., Mittal, R.R. and Mittal, R.K. (2002) A novel ultrasound technique to study the biomechanics of the human esophagus in vivo. *Am. J. Physiol. Gastrointest. Liver Physiol.* **282** : G785-G793. [DOI: 10.1152/ajpgi.00394.2001](https://doi.org/10.1152/ajpgi.00394.2001)
- [27] Patel, D., Janicki, J. and Carew, T. (1969) Static anisotropic elastic properties of the aorta in living dogs. *Circulation Research*, Vol. **XXV** : 765-779. [DOI: 10.1161/01.res.25.6.765](https://doi.org/10.1161/01.res.25.6.765)
- [28] Nahon, D. and Lee, J. (1986) A two-dimensional incremental study of the static mechanical properties of vascular grafts. *Clinical Materials* **1**: 177-197.
- [29] Cox, R. (1975) Anisotropic properties of the canine carotid artery *in vitro*. *J. Biomechanics*, **8**: 293-300 .
- [30] Sugita, S., Kato, M., Wataru, F., Nakamura, M. (2019) Three-dimensional analysis of the thoracic aorta microscopic deformation during intraluminal pressurization. *Biomechanics and modeling in mechanobiology*. <https://doi.org/10.1007/s10237-019-01201-w>
- [31] Skacel, P. and Bursa, J. (2022) Poisson’s ratio and compressibility of the arterial wall-improved experimental data reject auxetic behavior. *Jour. Mech. Behav. BioMed. Mat.* **131**: 105229. <https://doi.org/10.1016/j.jmbbm.2022.105229>
- [32] Holzapfel, G., Gasser, T. and Ogden, R. (2000) A new constitutive framework for arterial wall mechanics and a comparative study of material models. *J. Elast. Phy. Sci. Solid*, **61(1)**, 1-48. <https://doi.org/10.1023/A:1010835316564>